

## Article

# Hydrodynamic Processes Controlling Sand Bank Mobility and Long-Term Base Stability: A Case Study of Arklow Bank

Shauna Creane <sup>1,2,3,\*</sup> , Michael O'Shea <sup>1,2</sup> , Mark Coughlan <sup>3,4,5</sup>  and Jimmy Murphy <sup>1,2</sup> <sup>1</sup> School of Civil & Environmental Engineering, University College Cork, College Road, T12 K8AF Cork, Ireland<sup>2</sup> SFI Research Centre for Energy, Climate and Marine (MaREI), Beaufort Building, Environmental Research Institute, University College Cork, Ringaskiddy, P43 C573 Cork, Ireland<sup>3</sup> Gavin and Doherty Geosolutions, Unit A2, Nutgrove Office Park, Rathfarnham, D14 X627 Dublin, Ireland<sup>4</sup> School of Earth Sciences, Science Centre West, University College Dublin, Belfield, D04 N2E5 Dublin, Ireland<sup>5</sup> SFI Research Centre for Applied Geosciences (iCRAG), O'Brien Centre for Science East, University College Dublin, D04 N2E5 Dublin, Ireland

\* Correspondence: shauna.creane@ucc.ie

**Abstract:** Offshore sand banks are an important resource for coastal protection, marine aggregates, and benthic habitats and are the site of many offshore wind farms. Consequently, a comprehensive understanding of the baseline processes controlling sand bank morphodynamics is imperative. This knowledge will aid the development of a long-term robust marine spatial plan and help address the environmental instability arising from anthropogenic activities. This study uses a validated, dynamically coupled, two-dimensional hydrodynamic and sediment transport model to investigate the hydrodynamic processes controlling the highly mobile upper layer of Arklow Bank, while maintaining overall long-term bank base stability. The results reveal a flood and ebb tidal current dominance on the west and east side of the bank, respectively, ultimately generating a large anti-clockwise residual current eddy encompassing the entire bank. This residual current flow distributes sediment along the full length of the sand bank. The positioning of multiple off-bank anticlockwise residual current eddies on the edge of this cell is shown to influence east–west fluctuations of the upper slopes of the sand bank and act as a control on long-term stability. These off-bank eddies facilitate this type of movement when the outer flows of adjacent eddies, located on both sides of the bank, flow in a general uniform direction. Whereas they inhibit this east–west movement when the outer flows of adjacent eddies, on either side of the bank, flow in converging directions towards the bank itself. These residual eddies also facilitate sediment transport in and out of the local sediment transport system. Within Arklow Bank's morphological cell, eight morphodynamically and hydrodynamically unique bank sections or 'sub-cells' are identified, whereby a complex morphodynamic–hydrodynamic feedback loop is present. The local east–west fluctuation of the upper slopes of the bank is driven by migratory on-bank stationary and transient clockwise residual eddies and the development of 'narrow' residual current cross-flow zones. Together, these processes drive upper slope mobility but maintain long-term bank base stability. This novel understanding of sand bank morphodynamics is applicable to bedforms in tidally dominated continental shelf seas outside the Irish Sea.

**Keywords:** Arklow bank; hydrodynamics; sand bank morphodynamics; offshore renewable energy; sand bank stability; numerical modelling



**Citation:** Creane, S.; O'Shea, M.; Coughlan, M.; Murphy, J. Hydrodynamic Processes Controlling Sand Bank Mobility and Long-Term Base Stability: A Case Study of Arklow Bank. *Geosciences* **2023**, *13*, 60. <https://doi.org/10.3390/geosciences13020060>

Academic Editors: Katrien Van Landeghem and Jesus Martinez-Frias

Received: 8 December 2022

Revised: 20 January 2023

Accepted: 10 February 2023

Published: 17 February 2023



**Copyright:** © 2023 by the authors. Licensee MDPI, Basel, Switzerland. This article is an open access article distributed under the terms and conditions of the Creative Commons Attribution (CC BY) license (<https://creativecommons.org/licenses/by/4.0/>).

## 1. Introduction

Offshore linear sand banks are elongated sedimentary bedforms located in tidally dominated continental shelf seas. They are important features, providing a habitat for many epifaunal, infaunal and fish species [1–3], as a source of marine aggregates [4,5], and as sites for offshore renewable energy developments, for example, Scroby Sands Wind Farm

in the North Sea. Consequently, a comprehensive understanding of sand bank dynamics and stability is imperative for sustainable long-term marine spatial planning.

Arklow Bank, located off the south-east coast of Ireland, hosts Ireland's only presently constructed offshore wind farm (OWF) (Arklow Wind Park Phase 1), which is earmarked for further expansion (Arklow Wind Park Phase 2) [6] (Figure 1). Additionally, a number of OWFs are at the planning stage in the south-western Irish Sea, spread across the complex inter-related sediment transport pathways identified by Creane et al. [7]. Arklow Bank is proposed to have formed during the Early Holocene, during post-glacial marine transgression conditions, when a stronger-than-present hydrodynamic regime and abundant sediment supply supported the potential for submarine bedform formation [8–13]. The glacial and post-glacial sediments comprising the bank and its surroundings continue to be modified and re-worked by modern-day hydrodynamics [14–17]. Although the positioning of Arklow Bank (approximately 27.5 km in length and 1–2 km in width) is relatively stable over a long-term period [13,18], it hosts an upper highly mobile layer of surficial sandy sediments (medium to coarse sand) [7,14,18,19]. Coughlan et al. [14] developed a mobilisation frequency index (MFI) to calculate the yearly exceedance of critical bed shear stress under pure current, pure wave, and combined current and wave-induced bed shear stress. Notably, areas of the Arklow Bank display an MFI of 55% to 70% under both pure current and combined current and wave-induced bed stress. Only restricted parts of the bank display an exceedance of the critical bed shear stress under solely wave conditions, with an MFI of approximately 10% to 15%.

Global and local scour are important engineering challenges in offshore wind farm design. Global scour is overall seabed movement, including migrating sand waves and sand banks, whereas local scour is erosion around a foundation caused by the formation of horseshoe vortices around the pile in a flow. Scour influences the bearing capacity of the monopile foundation and the dynamic behaviour of the structure and thus could cause structural instability. Therefore, the ability to accurately predict natural seabed level change and local scour depth are important prerequisites to the calculation of design loads and the determination of an optimized embedment depth of the monopile. This knowledge also informs the selection of optimal mitigation strategies, which will ultimately reduce project cost and risk. During the development of Arklow Wind Park Phase 1, turbine locations on the bank were prone to the development of local scour, which led to infrastructural instability, resulting in mitigation measures to be put in place [20,21]. However, relatively little is known about the magnitude of the natural bed level changes along the length of Arklow Bank and the underlying processes that drive bank seabed mobility yet maintain overall bank base stability. This will be an important challenge to consider for Arklow Wind Park Phase 2.

Creane et al. [7] show that Arklow Bank obliquely aligns to the prevailing tidal flow, giving rise to a flood–ebb tidal dominance on either side of the bank. This characteristic compares with other linear sand banks across the northern hemisphere [8,13,22,23]. The nature of this tidal dominance is ultimately reflected in sand wave dynamics, where recent studies show that on the south-eastern side of the bank, sand waves with a mean height and wave length of 3 m and 140 m, respectively, migrate southwards at mean rate of 23 m/y [7]. Contrastingly, sand waves on the south-western side of the bank display a mean height and wave length of 2.3 m and 123.5 m, respectively, and migrate northwards at a rate of 32.7 m/y [7] (Figure 1). Furthermore, sand wave analysis reveals the presence of a bed load convergence zone at the southern tip of Arklow Bank, indicating the limiting point of southward bed load sediment transport [7]. The convergence of a southward moving flow on the eastern side of the bank with a north-westward residual current flow coming from an offshore independent sand wave field located approximately 10 km south-east of Arklow Bank influences these bed load dynamics [7].

Creane et al. [7,13] show that Arklow Bank's local sediment transport system is linked with offshore sand deposits unattached to sand banks and the bed load parting zone in the central Irish Sea. During the flood tidal phase, the dominant  $M_2$  tidal wave enters the

Irish Sea through the North Channel and St. George’s Channel to the north and south, respectively. The complex rotation of these tidal waves around two amphidromic points (one real and one degenerate) causes an intersection of the tidal waves between Ardanary (52.860° N, 6.058° W) on the east coast of Ireland and Anglesey (53.248° N, 4.607° W) on the UK coastline [13]. This interaction generates a tidal symmetry zone (Figure 1), giving rise to a bed load parting zone (BLP) [13]. BLPs are areas of maximum bed shear stress [24,25] that mark the ‘head’ of divergent sediment transport pathways and hence are important components of the sediment dispersal regime on tidally dominated continental shelves. This BLP directly influences the sediment transport regime across the south-western Irish Sea, including Arklow Bank. Through the combined use of hydrodynamic modelling, repeat geophysical bathymetric surveys, theoretical parameters, and multiple environmental variables, Creane et al. [7] highlighted three residual circulatory transport pathways in the south-western Irish Sea, whereby sediment is recycled between offshore sand banks and offshore independent sand wave fields. Two of these systems include Arklow Bank, the details of which are discussed in Creane et al. [7]. Evidence is provided to support a semi-closed anticlockwise residual current flow around the bank, whereby potential external sediment source pathways are identified through modelled residual tidal currents. Adding to the complexity of this continental shelf sea’s oceanography, evidence to support the presence of a semi-diurnal tidal node oscillation zone on the south-east coast of Ireland is presented by Creane et al. [13], from which tidal ranges increase outwards from this location across the Irish Sea (Figure 1).

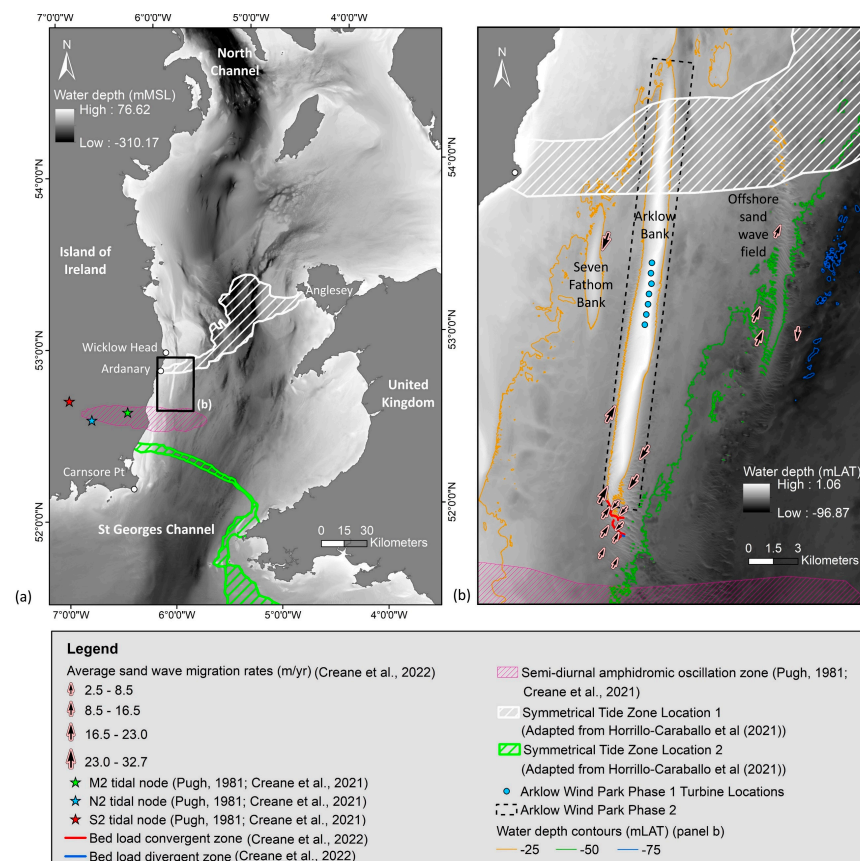


**Figure 1.** (a) Overview of Irish Sea oceanographic phenomena impacting the study site [7,13,23,26]; (b) the area of interest, Arklow Bank. Panel (a) bathymetry source: EMODnet [27], where MSL is mean sea level; Panel (b) bathymetry source: INFOMAR (<https://www.infomar.ie/>, (accessed on 20 March 2020)), where LAT is lowest astronomical tide.

This study will focus on addressing the following hypothesis: the upper mobile layer of Arklow Bank and the long-term bank base stability are controlled by the positioning of residual current eddies on and around this bedform.

From this, three research questions will be addressed:

1. How do the hydrodynamic processes and bank mobility vary along the length of Arklow Bank?
2. What are the underlying hydrodynamic processes driving this variation?
3. What hydrodynamic phenomena control the bank’s long-term stable positioning?

Addressing these research questions is critical in order to reduce risk in the detailed design of wind farm foundations, export cables [28] and associated protection structures [29], but also to aid the understanding of these bank systems in order to conserve benthic habitats and reduce the risk of environmental instability due to anthropogenic seabed disturbances. Knowledge derived from this study can be applied to other tidally dominated sand bank systems around the globe.

## 2. Methodology

A dynamically coupled two-dimensional (2D) hydrodynamic and sediment transport model was developed using DHI’s MIKE 21 suite of tools [30,31]. The setup of the model is detailed in Creane et al. [32] and provided as supplementary material to this article along with validation details for water levels, currents and suspended sediment transport. Notably, Creane et al. [32] successfully validate the suspended sediment transport component of the 2D model using three newly tested model validation techniques. The locations of the collected ADCP-based suspended solids concentration ( $SSC_{solids}$ ) dataset and water sample-based  $SSC_{solids}$  stations are displayed in Figure 2.

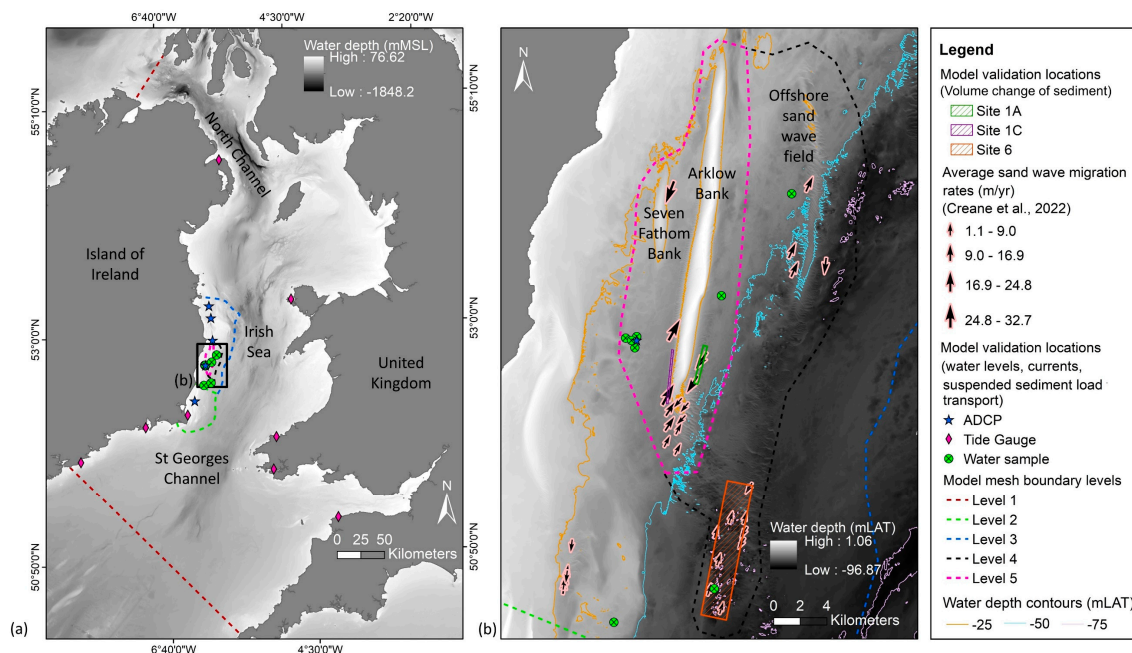


**Figure 2.** (a,b) Numerical model boundaries, mesh resolution levels and validation points [7,32]. Panel (a) bathymetry source: EMODnet [27] where MSL is mean sea level; Panel (b) bathymetry source: INFOMAR (<https://www.infomar.ie/>, (accessed on 20 March 2020)), where LAT is lowest astronomical tide.

For this study, the levels of resolution of the unstructured triangular flexible mesh are increased from four to five. The five levels of resolution are defined as (Figure 2):

- Level 5: 50 to 80 m over Arklow Bank and Seven Fathom Bank;

- Level 4: 150 to 200 m, encompassing the Arklow Bank system, including offshore independent sand wave field identified in Creane et al. [7];
- Level 3: 500 m to 600 m buffer zone, extending from the approximate  $-70$  m water depth contour to the coastline from Howth Head ( $53.37861^\circ$ ,  $-6.057222^\circ$ ) to Courtown ( $52.645^\circ$ ,  $-6.228333^\circ$ ), and covering any sand banks outside these areas off the south-east coast of Ireland;
- Level 2: 800 m to 1000 m, extending along the  $-70$  m contour to the coast from Courtown to Carnsore Point ( $52.17056^\circ$ ,  $-6.355278^\circ$ );
- Level 1: 2500 m to 3000 m resolution for the rest of the model domain.

The set-up of the sediment transport model is consistent with Creane et al. [32]. As in Creane et al. [32], artificial samples were placed in areas where a significant deficit of measured samples was evident, in order to produce the most realistic interpolated dataset when comparing against coarse seabed substrate maps, such as the EMODnet seabed substrate map [33]. In this case, a constant  $D_{50}$  value of 0.7 mm, which correlates with coarse sand according to the Wentworth scale [19], characterizes Arklow Bank.

As there were no publicly available time-lapse bathymetry datasets extending across the upper bank, validation of simulated bed levels across the bank could not be carried out. Instead, volumetric analysis of repeat bathymetry datasets and simulated bed level changes was carried out in areas where limited repeat bathymetry data were available. Three different sites were assessed (Figure 2), whereby targeted repeat bathymetry datasets were collected during three offshore research survey campaigns (CV20010, CV21034 and CV21035) under the research project ‘Mobility of Sand Waves and Sediment Banks (MOVE) Phase 1 and Phase 2’ [7]. These sites are numbered 1a, 1c and 6 as per the nomenclature in Creane et al. [7]. For each site, two bathymetry datasets were utilized. The volume of sediment above a certain reference level was first calculated from the earliest measured bathymetry dataset, followed by the later measured bathymetry dataset. The measured volume change over this time period between the two surveys was calculated (Table 1). Simultaneously, the earliest bathymetry dataset was interpolated to the model mesh, and a simulation was run to predict bed levels for the second time-stamp using a time step of 30 s. The volume of sediment was then calculated above a certain reference level from the interpolated bathymetry dataset and then from the final simulated bed level. The simulated volume change over this time period was calculated. A comparison between measured and modelled volume change was carried out. All three analysed sites present a variance between measured and simulated bed levels of less than 1.1% (Table 1).

**Table 1.** Comparison of simulated bed level changes against measured repeat bathymetry datasets at different sites in the model domain.

Site	Location	Data Type	Date of Survey; Simulation Start/End Date	Overlap Surface Area (km <sup>2</sup> )	Volume Change $\Delta V$ (%)	Variance (%)
6	8 km south-east of Arklow Bank	Measured bathymetry	27 September 2020	19.7	+3.5	0.2
			06 December 2021			
		Modelled bed level	27 September 2020			
			06 December 2021			
1A	South-eastern side of Arklow Bank	Measured bathymetry	10 October 2020	0.7	+0.6	1.1
			30 March 2021			
		Modelled bed level	10 October 2020			
			30 March 2021			
1C	South-western side of Arklow Bank	Measured bathymetry	10 October 2020	0.5	+1.8	0.8
			30 March 2021			
		Modelled bed level	10 October 2020			
			30 March 2021			

This coupled hydrodynamic and sediment transport model was run over a typical one-year period (12 lunar month tidal cycles) from September 2020 to September 2021 to analyse the interaction between tidal current dynamics and morphological changes over this time scale.

### 3. Results and Discussion

#### 3.1. General Bank Morphodynamics from a Flood-Neap Tidal Cycle to Full Lunar Cycle

In order to assess bank morphodynamics over a flood-neap tidal cycle, simulated bed level changes were calculated over two 6-h slack to slack tidal phases, ending directly after a flood tide and an ebb tide. From Figure 3a,b, it is clear that the upper bank migrates from west to east and east to west over the flood and ebb tidal phases, respectively, due to the nature of the cross-flows during each tidal phase [34]. Peak flood and peak ebb currents over this time period are presented in Figure 4. Over this time period, the bank moves in the same direction along the full length of the bank, with the exception of at least three morphologically 'stable' zones. These stable zones correlate with relatively shallow areas of the bank (<3 mMSL). The maximum erosion over the flood and ebb tidal phases is  $-0.32$  m and  $-0.33$  m, respectively, and the maximum accretion is  $+0.29$  m and  $+0.76$  m.

Analysis of bed level changes over a flood-ebb (Figure 3c), spring-neap (Figure 3d) and one lunar month tidal cycle (Figure 3e) reveals an inconsistent pattern of tidal dominance along the length of the bank, separating the bank into morphological sections. From the northern tip moving southwards in Figure 3e, an approximate 3.3 km section of the bank crest migrates westwards. Next, an immobile zone dominates for approximately 800 m, followed by a successional eastward, westward, eastward, westward migration over an 8 km section of the bank. Another stability zone is then observed for approximately 1 km, followed by 4 km of eastward migration and 600 m of stability, until finally, eastward migration again dominates over a 5.8 km section of the bank. These upper bank migration patterns coincide with the direction of tidal asymmetry presented in Figure 5a–c.

The impact of tidal asymmetry on upper bank migration patterns remains evident over a one-year simulation period (e.g., Figure 3e–g). However, Figure 3h,i shows that the nature of each individual lunar month's dynamics are different from one another, whereby over the mobile sections, erosion occasionally takes place in a previously noted accretion zone and vice versa. This suggests that tidal current residuals alter from month to month, dynamically adjusting in strength and direction, with a constant change in bank morphology. As a result, although Figure 3g reveals relatively large bed level changes along the bank (ranging from  $+14.5$  m to  $-11$  m), the direct comparison of  $t_{12mo}$  bed levels to  $t_0$  bed levels fails to capture the morphological changes of the sand bank occurring over shorter timescales within this one-year period (as highlighted in Figure 3h,i). Thus, a maximum bed level change of  $+14.5$  m and  $-11$  m over this time period (Figure 3g) does not represent direct accretion or erosion; instead, these are resultant net changes after continuous upper bank east–west fluctuation over time. Additionally, as the upper bank fluctuates in an east–west migration pattern, bed level changes occur from the shift in bank slope positioning over time rather than solely traditional erosion and accretion processes. Therefore, bed level changes represented along the sand bank comprise the resultant changes due to the shift in bank slope positioning and due to traditional erosion and accretion processes and therefore must be interpreted with caution.

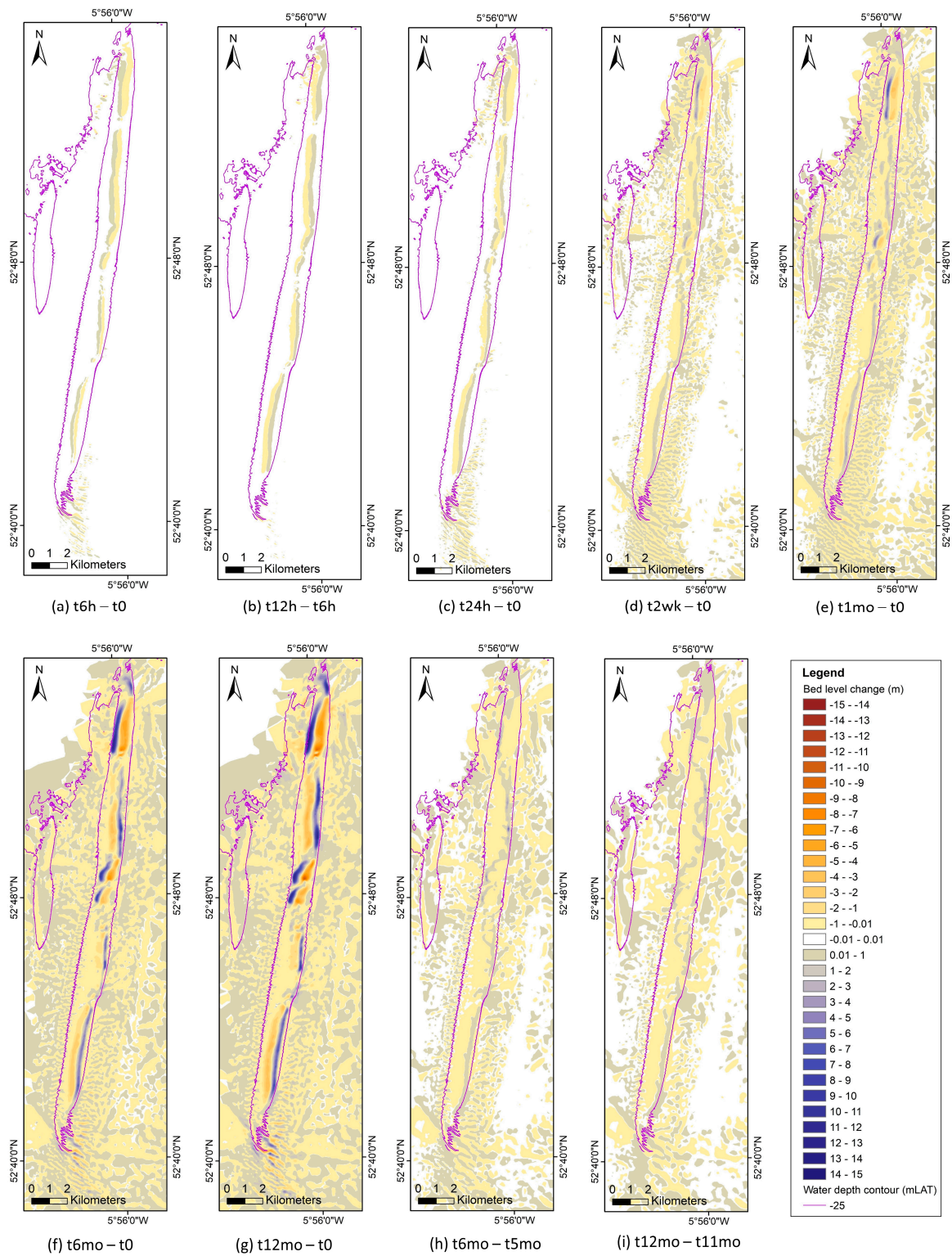


**Figure 3.** Bed level changes at Arklow Bank over various time periods calculated from extracted simulated bed levels; (a) after one ebb tidal phase, (b) after one flood tidal phase, (c) after two ebb and two flood tides, (d) after one spring-neap cycle, (e–g) after 1, 6 and 12 lunar month simulations, (h–i) after one spring-neap cycle between simulation months 5 and 6, and 11 and 12, respectively. A  $-25$  m water depth contour is provided based on INFOMAR bathymetry data referenced to Lowest Astronomical Tide (LAT). INFOMAR data available at: <https://www.infomar.ie/>, (accessed on 20 March 2020).

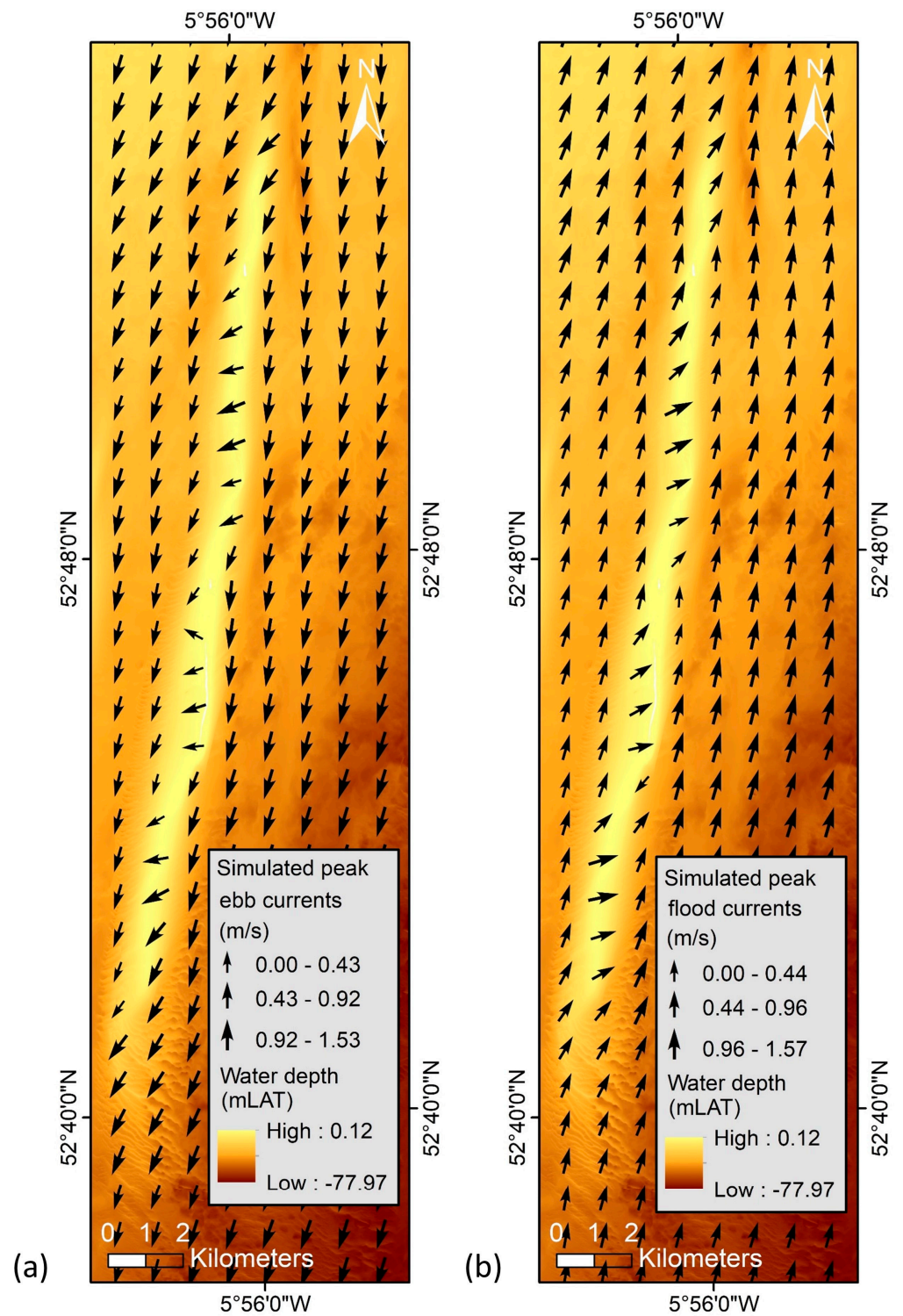
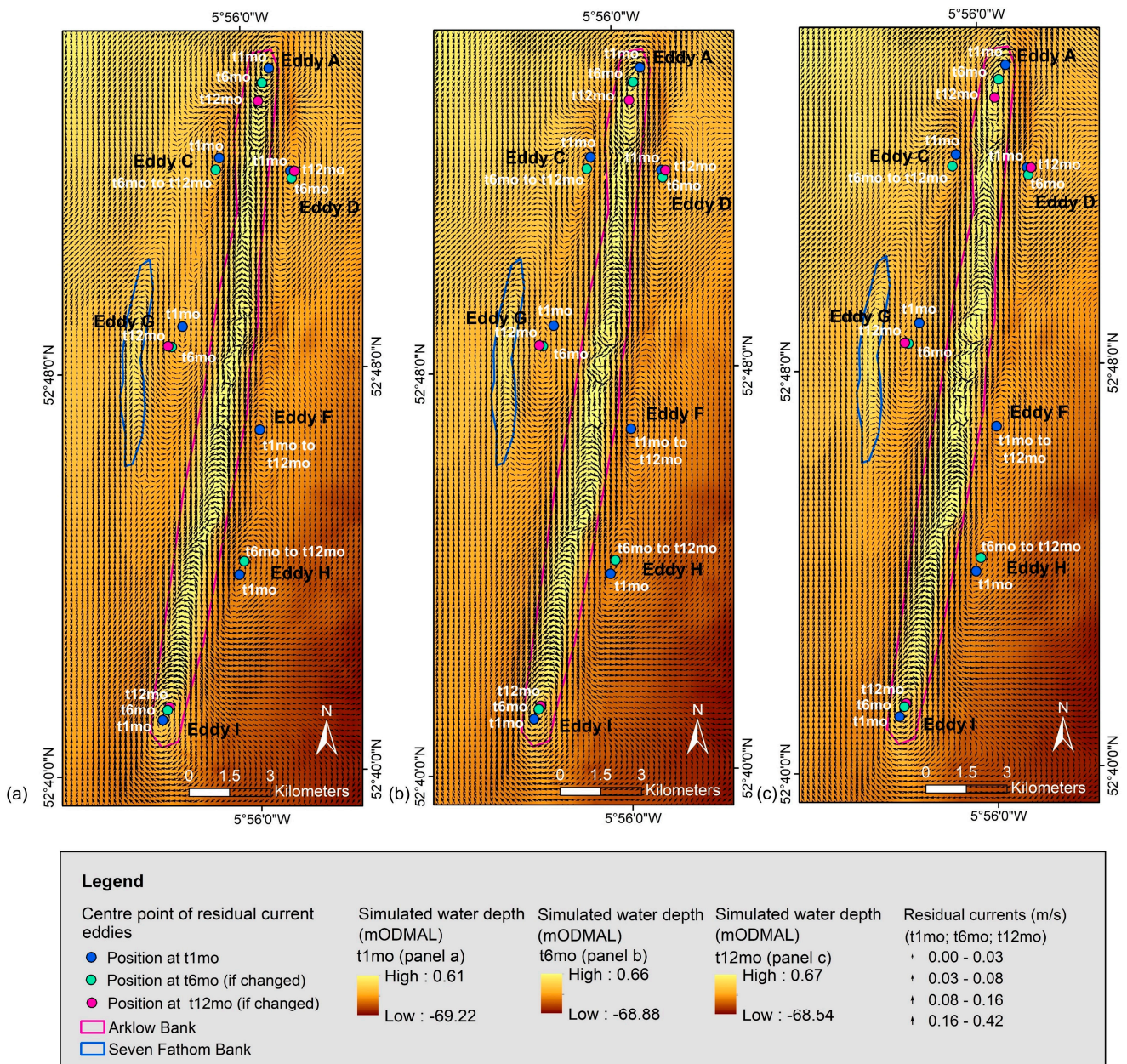


Figure 4. (a,b) Simulated peak ebb and flood depth-averaged currents, respectively. Bathymetry source: INFOMAR (<https://www.infomar.ie/>, (accessed on 20 March 2020)).



**Figure 5.** Simulated residual currents for the (a) first (t1mo), (b) sixth (t6mo) and (c) twelfth (t12mo) month of a one-year simulation period. Simulated bed levels at the end of each simulated month are also presented; t1mo is the simulated bed level at the end of the first month.

To investigate this east–west morphodynamic fluctuation, the residual tidal currents for each lunar month over a 12-month period were calculated (Figure 5). Hereafter, each lunar month cycle will be referred to as ‘tXmo’, with the first and twelfth lunar month cycles referred to as t1mo and t12mo, respectively. Similar to other offshore linear sand banks on the European continental shelf [8,34], the first lunar month’s residual tidal currents reveal a strong flood (northward) and ebb (southward) dominance on the western and eastern side of the bank, respectively (Figure 5a–c). This correlates well with sand wave migration dynamics on either sides of the bank [7] (Figure 1b). Clearly, a strong, anticlockwise residual current eddy encompasses the bank, suggesting a semi-closed sediment transport system. Multiple off-bank anticlockwise residual current eddies are pinpointed on the outside of this cell (Figure 5a–c), including a complex partial anticlockwise curvilinear flow originating from Seven Fathom Bank (Eddy G in Figure 5a–c). Additionally, a number of clockwise

residual eddies are distributed along the length of the bank, the most prominent being Eddy A and Eddy I, illustrated in (Figure 5a–c). These eddies are intermittent, with regions of strong residual cross-flows and areas of limited cross-flows. For each lunar month up to the 12th lunar month, similar features are noted with slight variations, reiterating the potential for a hydrodynamic–morphodynamic feedback system along the length of the bank. This is evident in Figure 5a–c, where the migration of the eddy centres from t1mo to t6mo to t12mo are pinpointed. These notable monthly variations in bed levels and residual currents are discussed in more detail in Section 3.2.

### 3.2. Detailed Analysis of Hydrodynamic–Morphodynamic Feedback Loop

From the combined cross-sectional analysis of simulated monthly bed levels and monthly variation in residual tidal currents, a complex morphodynamic–hydrodynamic feedback system is evident. Clearly, the development and migration of both clockwise and anticlockwise residual current eddies both on and off the bank, and associated residual tidal flows, are directly linked to both east–west migration patterns of the bank and vertical erosion/accretion patterns. To present and discuss the variation of this phenomenon along the length of the bank, the bank will be split into eight sub-cells, which directly link to natural changes in the morphodynamic–hydrodynamic system.

#### 3.2.1. Sub-Cell 1

The morphodynamics of sub-cell 1 (Figure 6), the most northern sub-cell, are highly linked to

4. a clockwise on-bank residual current eddy (Eddy A) that migrates southwards,
5. the development of a clockwise on-bank residual current eddy (Eddy B) at the southern extent of this sub-cell, and
6. a morphodynamic stability point controlled by two off-bank, adjacent, anticlockwise residual current eddies (Eddy C and Eddy D).

At t1mo, the centre of the northern most clockwise residual eddy, hereafter referred to as Eddy A, lies approximately over cross-section L5 (Figure 6a). Tracking the location of the centre of Eddy A over the one-year simulation period reveals a continuous southwards migration of approximately 1.3 km. At t12mo, it lies approximately between L11 and L14. Due to the circular nature of this clockwise residual current eddy, the dominant cross-flow over the bank is eastwards and westwards, respectively, directly north and south of the centre of the eddy. Consequently, as the centre of Eddy A shifts southwards, the nature of the surrounding flow vectors subsequently adjusts.

In particular, the northern tip of the bank, an area outside the migration route of Eddy A's centre, shows evidence of residual current vector adjustment, which directly impacts the morphodynamic response of the bank. Over this northern tip of the bank, observations show a simultaneous reduction in residual current magnitudes and consistent rotation of the eastward current vectors southward, as Eddy A migrates south (Figure 6a). Cross-sections L0 to L4 highlight the existing hydrodynamic–morphodynamic feedback loop, whereby the bank crest simultaneously migrates eastward and shallows (up to 7 m), ultimately aligning with the gradual rotation of residual current vectors, allowing a build-up of sediment on the upper slopes and crest (Figure 6b). Additionally, the gradual development of a southward flow on the east side of the bank acts as a limitation to accretion on the eastern slope and a barrier to further eastward migration; thus, accretion takes place mostly on the upper stoss slope or crest of the bank.

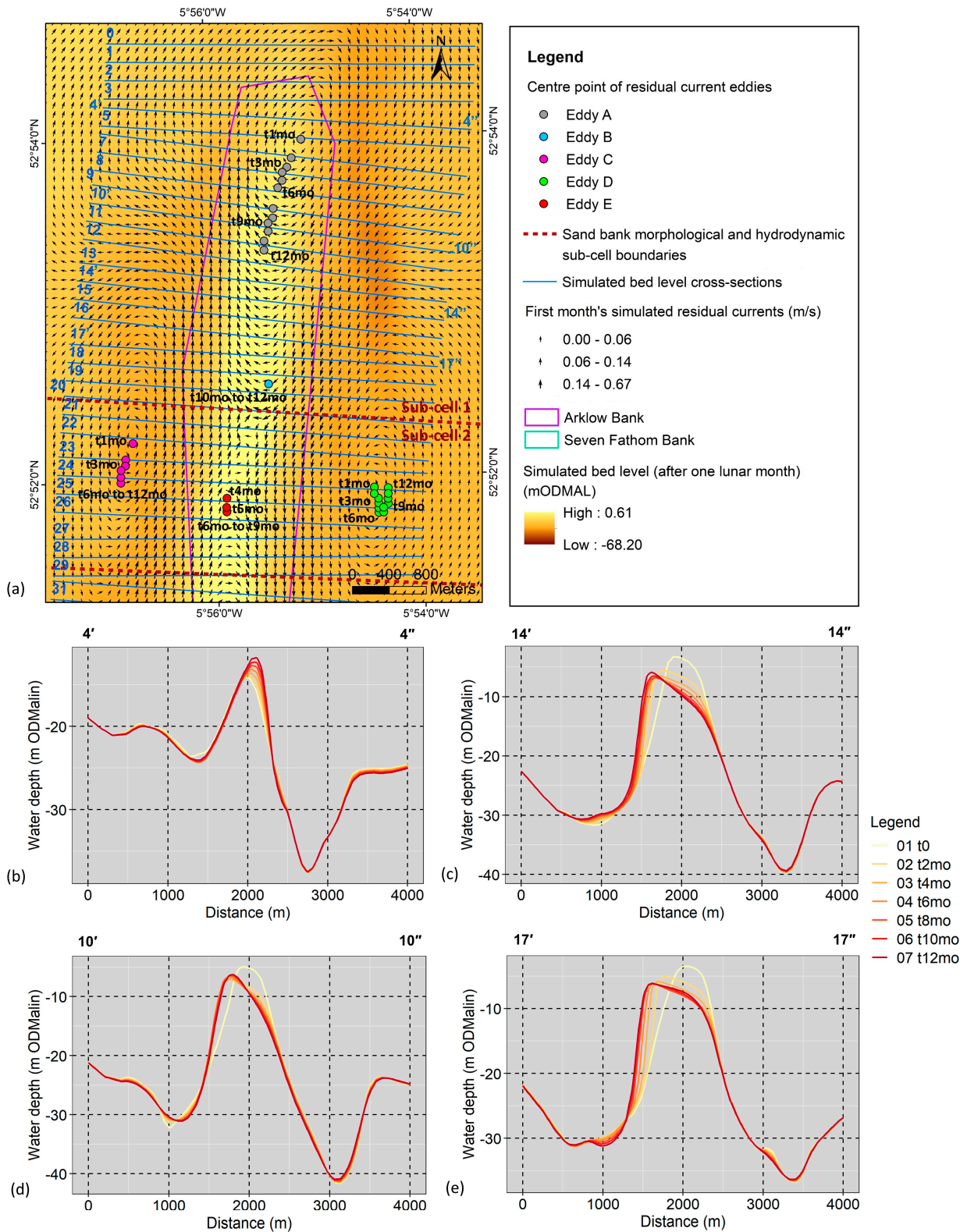


**Figure 6.** Morphodynamics and hydrodynamics at Sub-cell 1 of Arklow Bank. (a) Simulated bed level change after one lunar month and associated residual current vectors, overlain by the location of the centre point of residual eddies from residual currents during each subsequent lunar month simulation; ‘t6mo’ is the sixth lunar simulation month. (b–e) Simulated bed level over a one-year simulation at cross-sections 4, 14, 10 and 17; ‘t0’ is the starting bed level, and ‘mo’ is subsequent months.

Over a longer simulation period, the continuous rotation of these vectors at the northern tip of the bank suggests the formation of another on-bank clockwise residual eddy. In this way, as Eddy A develops and migrates southwards, another eddy develops in its place, ultimately acting as a conveyor belt of continuous migratory clockwise residual current eddies dynamically responding to and influencing the east–west morphodynamics of the bank.

Over the one-year period, the upper bank from L5 to L12 shifts migratory direction from westwards to eastwards, as the centre of Eddy A and the associated outer ring flows migrate southwards across these cross-profiles (Figure 6a,d). The centre of the eddy signifies a reduction of tidal residuals and an area of tidal symmetry, indicating potential for sediment accretion. Therefore, as the eddy migrates south over one point along the bank, a progressive morphodynamic response should be evident in the cross-sectional profiles; these include (i) a westward migration of the bank, (ii) slowing of east–west migration in conjunction with sediment accretion, i.e., increased bed levels, and finally (iii) eastward migration of the bank. This is evident in cross-sections L5 to L12 (Figure 6a,d). As expected, the timing of the shift in migration direction varies along the length of this section of the bank, progressing through cross-sectional lines L5 to L12, aligning directly with the continuous progression of the centre of the residual eddy southwards. Whilst the mobility of the bank varies from above the  $-15$  m contour to above the  $-25$  m contour in some areas of the bank, the base of the bank remains relatively stable over time.

Furthermore, L13 to L14 only display morphodynamic responses (i) and (ii), whereby the slowing of westward crest migration and coincident sediment accretion at approximately  $t_{10mo}$  and  $t_{12mo}$  align with the ending position of the centre of the residual eddy (Figure 6a,c).

Directly south of this region, approximately located between L15 to L19, at  $t_{6mo}$  there is a noticeable shift in the westward residual cross-flow to a north-westward direction. From  $t_{6mo}$  to  $t_{9mo}$ , a continuous clockwise rotation of these residual current vectors is noticeable, coinciding with the southward migration of Eddy A, until the full formation of Eddy B at  $t_{10mo}$  (Figure 6a). The centre of the eddy is located approximately between cross-sections L18 and L19. The coverage area of Eddy B is approximately 500 m to 700 m wide along the crest of the bank. The intersection between the northern-most eastward crossflow of Eddy B and the southern-most westward crossflow of Eddy A lies between L16 and L17 (Figure 6a,e). As a result of reduced magnitudes of residual currents and reduced extent of cross-flows both at (i) the centre of Eddy B and (ii) the intersection of Eddy B with Eddy A, this area is characterised by westward migration and erosion of up to approximately 2 m, directly followed by slowed migration and sediment accretion (Figure 6e). A temporary stability zone is evident due to these two hydrodynamic phenomena.

Sub-cell 1 is bound to the south by sub-cell 2, which is characterised by a morphodynamic stability point generated by the intersection of two off-bank anti-clockwise residual current eddies (Eddy C and Eddy D). This is described in detail in Section 3.2.2.

### 3.2.2. Sub-Cell 2

A clear hydrodynamic and morphodynamic transition point is evident from approximately L20 to L21 (Figure 7a). The southern-most westward residual cross-flows of Sub-cell 1 (including the outer-most ring of Eddy B) remain stable in terms of direction and positioning over this one-year period (Figure 7a). The southward shifting of these residuals is restricted by the dramatic change in bank morphology, shallowing from 5 to 10 m below mean sea level (MSL) to close to MSL. This shallow, symmetrical structure of the bank continues for circa. 800 m. Notably, relatively low mobility and high stability is observed in cross-sections L21 to L24 over the one-year time period (Figure 7b). At L25 and L26, the bank deepens in comparison to this first 800 m zone to approximately 3 m below MSL. However, a relative low mobility and high stability is still evident in bank morphology for approximately another 750 m (L25 to L29) (Figure 7c).

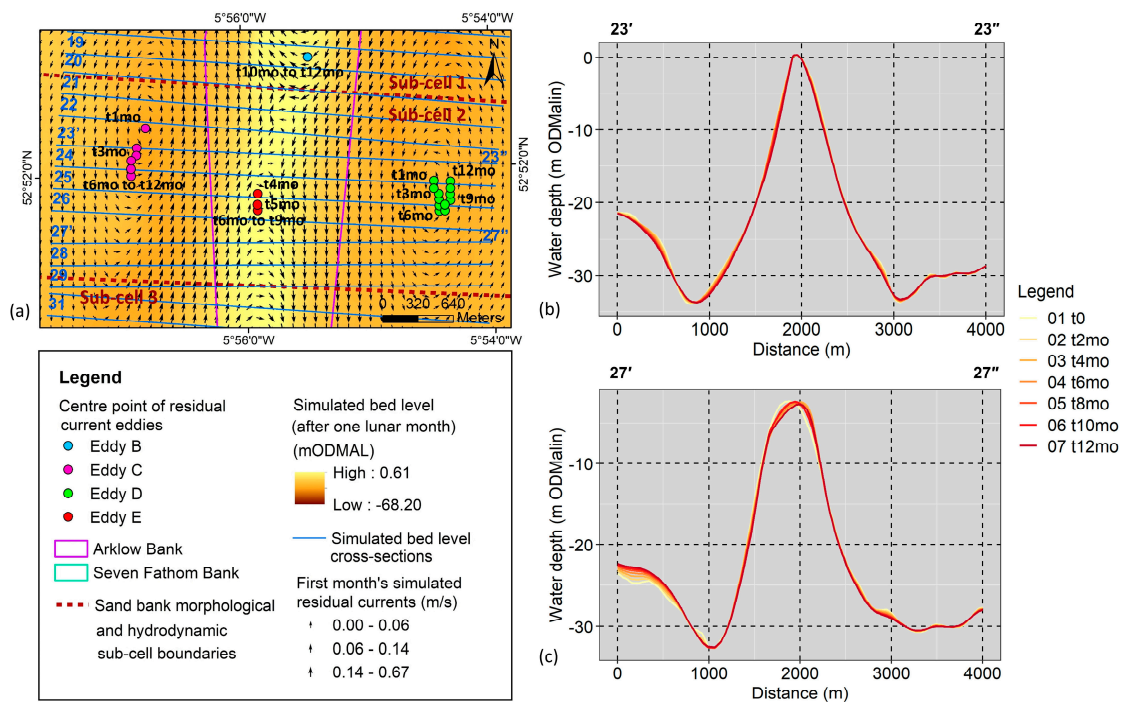


**Figure 7.** Morphodynamics and hydrodynamics at Sub-cell 2 of Arklow Bank. (a) Simulated bed level change after one lunar month and associated residual current vectors, overlain by the location of the centre point of residual eddies from residual currents during each subsequent lunar month simulation; ‘t6mo’ is the sixth lunar simulation month. (b,c) Simulated bed level over a one year simulation at cross-sections 23 and 27; ‘t0’ is the starting bed level, and ‘mo’ is subsequent months.

The maintenance of this ~1550 m morphological stability zone is driven by the presence of two anticlockwise residual current eddies located adjacently on the eastern and western side of the bank, respectively. These will hereafter be referred to as Eddy C and Eddy D (Figure 7a). The intersection of these eddies occurs along the crest/upper slopes of the bank, directly limiting residual cross-flows at very shallow areas and reducing both the width and magnitude of the cross-flows in other areas along this section. This ultimately reduces east–west fluctuation of the bank crest and increases the potential for sediment accretion/bank stability.

Unlike the transient and migratory nature of the on-bank clockwise residual current eddies identified in Sub-cell 1, the existence of these off-bank eddies remains constant throughout the simulation period. The positioning of the centre of Eddy C and D also remain relatively stable over time (Figure 7a). For example, from t1mo to t6mo, Eddy C migrates southwards by approximately 450 m, where it remains in the same location from t6mo to t12mo. On the other hand, Eddy D migrates approximately 280 m southwards from t1mo to t6mo. From t6mo to t12mo, it gradually migrates back up north, close to its original position (Figure 7a).

The first 800 m of the on-bank intersection of Eddy C and Eddy D, where the bank is at or above MSL, show little impact from these minor migration patterns; the length and position of the stability zone remains relatively constant over the same time period (Figure 7a,b). At the transition zone to the southern half of Sub-cell 2, the deepening of the bank permits an increase in current-driven mobility at this location. A relatively weak on-bank transient eddy (Eddy E) forms and disappears over time, corresponding to the movements of Eddy D, influencing a shift in crest migration from eastwards to westwards over a small section of the bank (L25–L27) (Figure 7a,c).

Overall, observations show that the general conveyor belt of clockwise on-bank residual current eddies tends to drive the east–west fluctuation of the bank in Sub-cell 1. This area of mobility is restricted and bound to the south by Sub-cell 2, a zone of relative stability,

ultimately maintained and driven by the stability of two off-bank anticlockwise residual current eddies.

### 3.2.3. Sub-Cell 3

Sub-cell 3 marks a transition to a region of high mobility (Figure 8a). Initially, eastward migration of the upper bank profile dominates the length of the bank. When a maximum 'threshold' of eastward asymmetry is reached, westward migration ensues. Unlike Sub-cell 1, on-bank residual eddy formation is absent. Instead, the reversal of crest migration direction correlates with increasing and decreasing width of westward residual cross-flows, combined with partial rotation of residual current vectors southward and northward on the eastern and western side of the upper slopes of the bank, respectively. Although a full rotation of vectors forming an eddy is absent, this reduction in width of the cross-flow and the rotation of current vectors on either side of the bank stimulate migration of the upper bank in the opposite direction, while the base of the bank remains stable. Reduced current magnitudes facilitate sediment accretion both at the crest and on the stoss slope, whilst the new southern flow stimulates erosion on the east side of the bank and inhibits further eastward migration. In this way, the bank migrates back towards a more symmetrical shape. Clearly, a morphodynamic–hydrodynamic looped response system controls the east–west fluctuation of the crest while maintaining bank base stability.

Over the one-year time period, most of Sub-cell 3 is dominated by an eastward residual cross-flow between 400 and 600 m wide. The area of reduced cross-flow (approximately 100 m wide), outlined previously, hereafter will be referred to as a 'narrow' area. This narrow area coincides with bank rejuvenation and intermittently moves to different areas of the bank over the one-year period. As the narrow area moves, the wider cross-flow replaces it and dominates that same area once again. The migratory nature of this 'narrow' area over the one-year simulation period is illustrated in Figure 8a. A number of representative cross-sectional profiles presented in Figure 8c–f exhibit the expected morphodynamic response of (i) eastward migration, (ii) bank rejuvenation back towards a symmetrical shape (westward migration), and in some cases (iii) eastward migration once again. The variation in each cross-sectional profile follows the timeline of successional wide-narrow-wide residual current changes.

As there is evidence of a reversed migration pattern over the majority of Sub-cell 3, the slope of the bank at this transition point was analysed from monthly extracted simulated bed levels. Notably, at cross-sections L30, L33, L36 and L40, a shift in migration direction occurred when the upper slopes reached an angle of approximately  $5.5^\circ$  to  $6^\circ$  (Figure 8b). When this approximate angle is reached, a hydrodynamic response is stimulated that alters the upper slope's erosion–accretion regime, thus influencing the east–west fluctuation of the crest and the bank's shape. In this way, the slope angle of the upper bank acts as a 'threshold' that stimulates tidal residuals to alter and reverse upper bank migration in the opposite direction. As the analysed bed levels are 'snapshots' at monthly intervals, this threshold angle may vary. Although the bank alters its migration direction corresponding to a certain slope threshold, the maximum horizontal displacement of the crest, the maximum vertical bed level changes are difficult to quantify, even under pure current conditions. For example, cross-section L30 shows that the lee slope has the ability to reach this threshold angle multiple times during an overall eastward migratory direction over this one-year time period (Figure 8c). An oscillatory-type upper slope migration exists, whereby multiple 'reversals' in upper slope migration occur in an overall consistently eastward migration. Over this one-year time period, the maximum horizontal displacement along this cross-section is not reached. The timing of this process varies along the length of Sub-cell 3. Detailed analysis of simulated bed levels at each timestep would help to elucidate this process at a finer scale. Furthermore, although sediment transport in this area of the Irish Sea is predominately driven by tidal current, wind and wave conditions are known to influence sediment transport in shallow water; thus, their influence on the east–west fluctuation of the upper bank should be investigated in future studies. Sub-cell 3 is bound

to the south by the approximate southern limits of the outer flows of off-bank residual current eddies, Eddy C and D (Figure 8a).

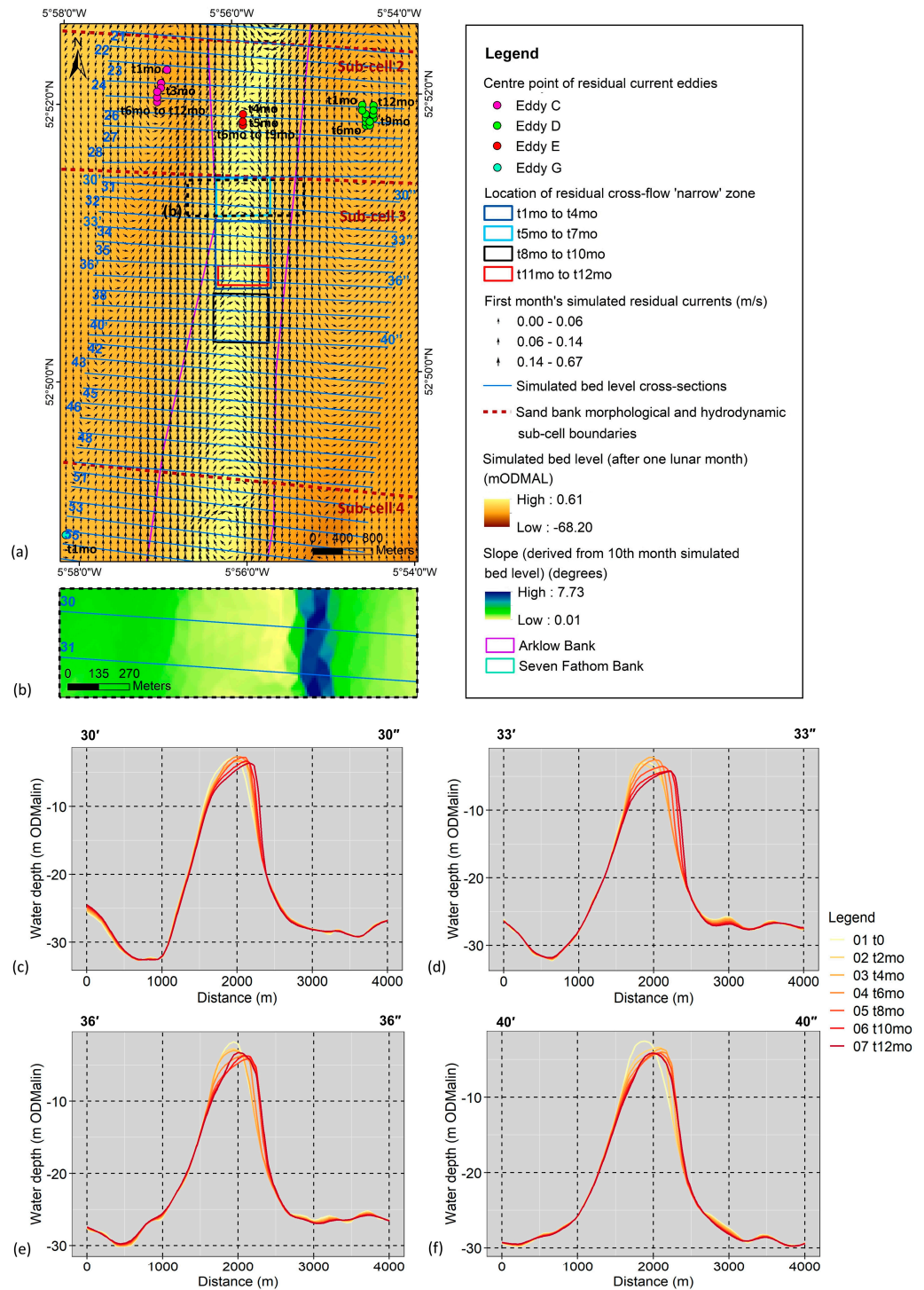


**Figure 8.** Morphodynamics and hydrodynamics at Sub-cell 3 of Arklow Bank. (a) Simulated bed level change after one lunar month and associated residual current vectors, overlain by the location of the centre point of residual eddies from residual currents during each subsequent lunar month simulation; 't6mo' is the sixth lunar simulation month. (b) Slope derived from the resulting bed level after 10 lunar month simulation, overlain by cross-section L30. (c–f) Simulated bed level over a one year simulation at cross-sections 30, 33, 36, and 40; 't0' is the starting bed level, and 'mo' is subsequent months.

### 3.2.4. Sub-Cell 4

Sub-cell 4 is longitudinally bound between the intersection point of the outer flows of Eddy D and Eddy F, and the approximate centre point of Eddy F (Figures 8a and 9a). The outer flows associated with the northern half of off-bank Eddy F drive westward and south-westward residual current flow toward the eastern side of the bank, potentially inhibiting the dominant eastward cross-flows originating from the western side of the bank. As a result, this region of the bank is characterised by a very complex morphodynamic and hydrodynamic regime driven by the interaction between this anticlockwise, off-bank residual eddy (Eddy F) on the eastern side of the bank, and the anticlockwise residual partial eddy-type flow (Eddy G) on the western side of the bank, located between Arklow Bank and Seven Fathom Bank (Figure 9a). The centre point of Eddy F maintains a relatively stable positioning over the 12-month simulation period. On the other hand, the centre point of the partial eddy, Eddy G, migrates 800 m south-westward from t1mo to t6mo, where it migrates an extra ~100 m in the same direction over the final 6-month time period (Figure 9a).

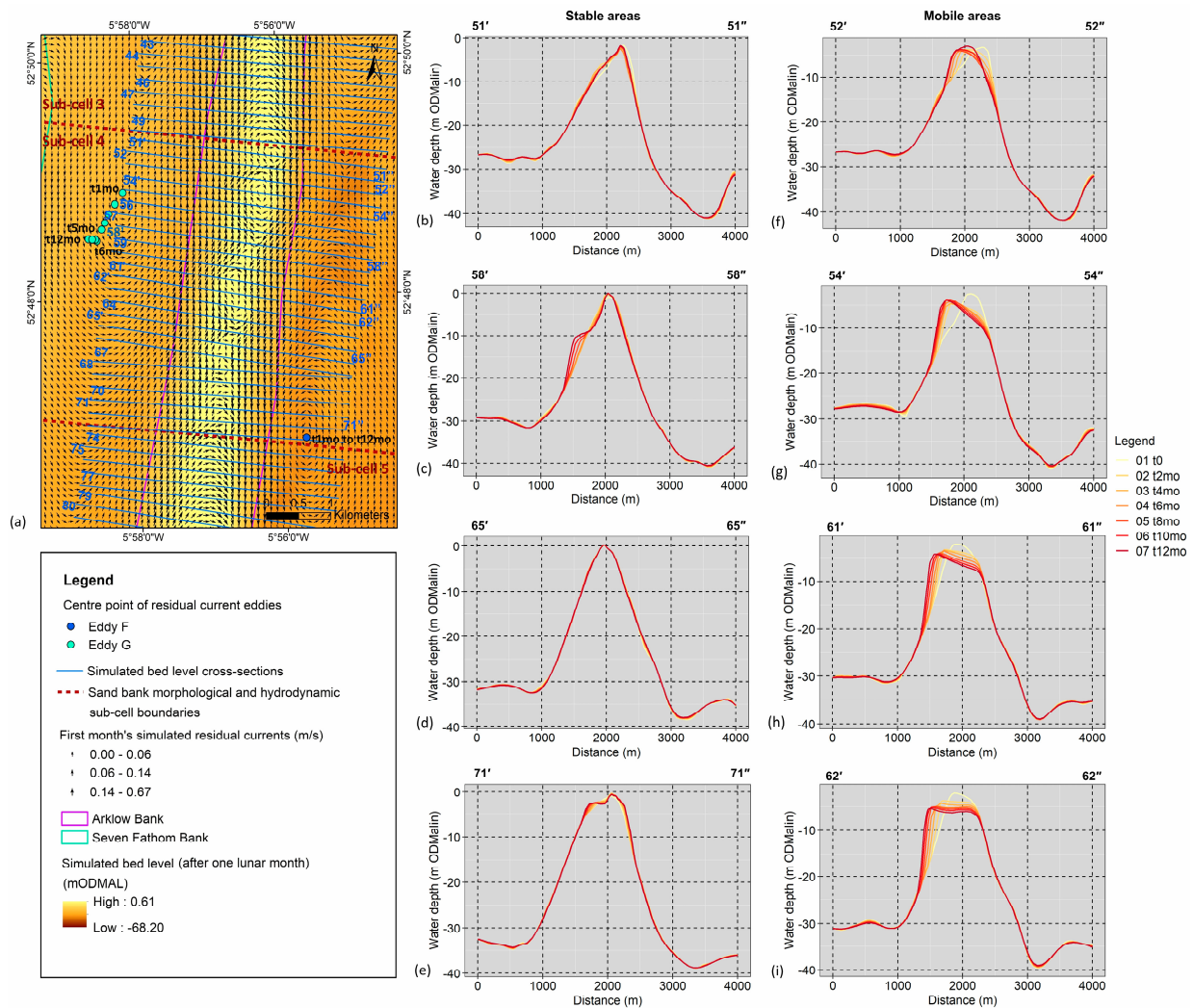


**Figure 9.** Morphodynamics and hydrodynamics at Sub-cell 4 of Arklow Bank. (a) Simulated bed level change after one lunar month and associated residual current vectors, overlain by the location of the centre point of residual eddies from residual currents during each subsequent lunar month simulation; ‘t6mo’ is the sixth lunar simulation month. (b–e) Simulated bed level over a one year simulation at cross-sections 51, 58, 65 and 71, representing ‘stable’ areas; ‘t0’ is the starting bed level and ‘mo’ is subsequent months; (f–i) cross-sections 52, 54, 61 and 62 representing ‘mobile’ areas.

The line of intersection of Eddy F and Eddy G gives rise to a complex hydrodynamic region of constant and transient on-bank clockwise residual eddies, where the centre point and the intersection point of the individual eddies are dominated by reduced residual current magnitudes and quantity of cross-flow. These points are intermixed with relatively higher eastward and westward residual cross-flows that increase outwards from the centre point of each eddy. This sequence of residual clockwise eddies along this section directly influences the morphodynamics of the bank, where areas displaying a symmetrical bank shape in combination with high upper bank stability and relatively shallow water conditions (ca. <3 mMSL water depth) (Figure 9a–e) alternate with relatively deeper water conditions (ca. >3 mMSL water depth) and lower upper bank stability regions (Figure 9a,f–i). Most notably, the relatively ‘stable’ areas over this one-year period are evident in cross-sections L51, L58–59, L64–69 and L71–72 (Figure 9b–e). These areas generally display very shallow morphology and align with the central point or intersections of the on-bank residual eddies. Over this time period, two notable regions show continuously high westward crest migration, geographically located over cross-sections L52–L56 (Figure 9f–g) and L60–L63 (Figure 8h–i). Given the long-term stable positioning of the bank, a longer simulation time period may highlight a threshold, as a result of which the westward crest migration is restricted and a reversal in crest direction is stimulated. In this way, the on-bank residual eddies might shift a few hundred metres to allow bank re-generation until the cycle re-starts.

### 3.2.5. Sub-Cell 5

An abrupt change in hydrodynamics and bank morphology is observed at the transition from Sub-cell 4 to Sub-cell 5 (Figure 10a). Notably, the upper bank deepens and transitions from a relatively symmetric to eastward asymmetric shape. This asymmetric shape and direction remain relatively stable over the one-year period for approximately 3 km of the bank, with sediment transport only causing minor vertical fluctuations (within  $\pm 2$  m bed level change) at the crest over the simulation period. This is visible in cross-sections L82–L86 (Figure 10a,b).

Modelled current residuals align with these morphological observations, with relatively consistent westward cross-flows noted. This hydrodynamic and morphodynamic consistent zone is pinpointed between the approximate centre point of Eddy F and the intersection of outer flows of Eddy F and Eddy H on the eastern side of the bank (Figure 10a). The curvilinear southward and south-eastward flows associated with the southern half of Eddy F on the eastern side of the bank generally do not converge against flows coming from the western side of the bank, opposite to that observed in Sub-cell 4. Instead, they align with the westward flows coming from the Seven Fathom Bank, partial Eddy G. In this way, instead of a tidal asymmetric, morphologically ‘stable’ zone developing along the upper bank, a consistent eastward bank asymmetry and eastward residual cross-flow is evident along this section. This shows that the existence and positioning of the off-bank residual eddies provide a strong control on long-term east–west fluctuation of the bank.

### 3.2.6. Sub-Cell 6

Similar to Sub-cell 2 and 4, the curvilinear south-westward, south-south-westward and southerly flows associated with the anticlockwise residual eddy, Eddy H, located on the eastern side of the bank, seems to inhibit westward cross-flows coming from the western side of the bank, ultimately generating another morphologically ‘stable’ zone (Figure 10a). Over the simulation period, the bank retains its symmetrical shape, and little to no crest mobility is evident (see cross-sections L90 to L93) (Figure 10a,c). The centre point of Eddy H remains relatively stable over the simulation period; it migrates northwards 500 m from t1mo to t6mo, where it remains in this position for t6mo to t12mo. This is a similar migratory pattern to Eddy C but in the opposite direction.

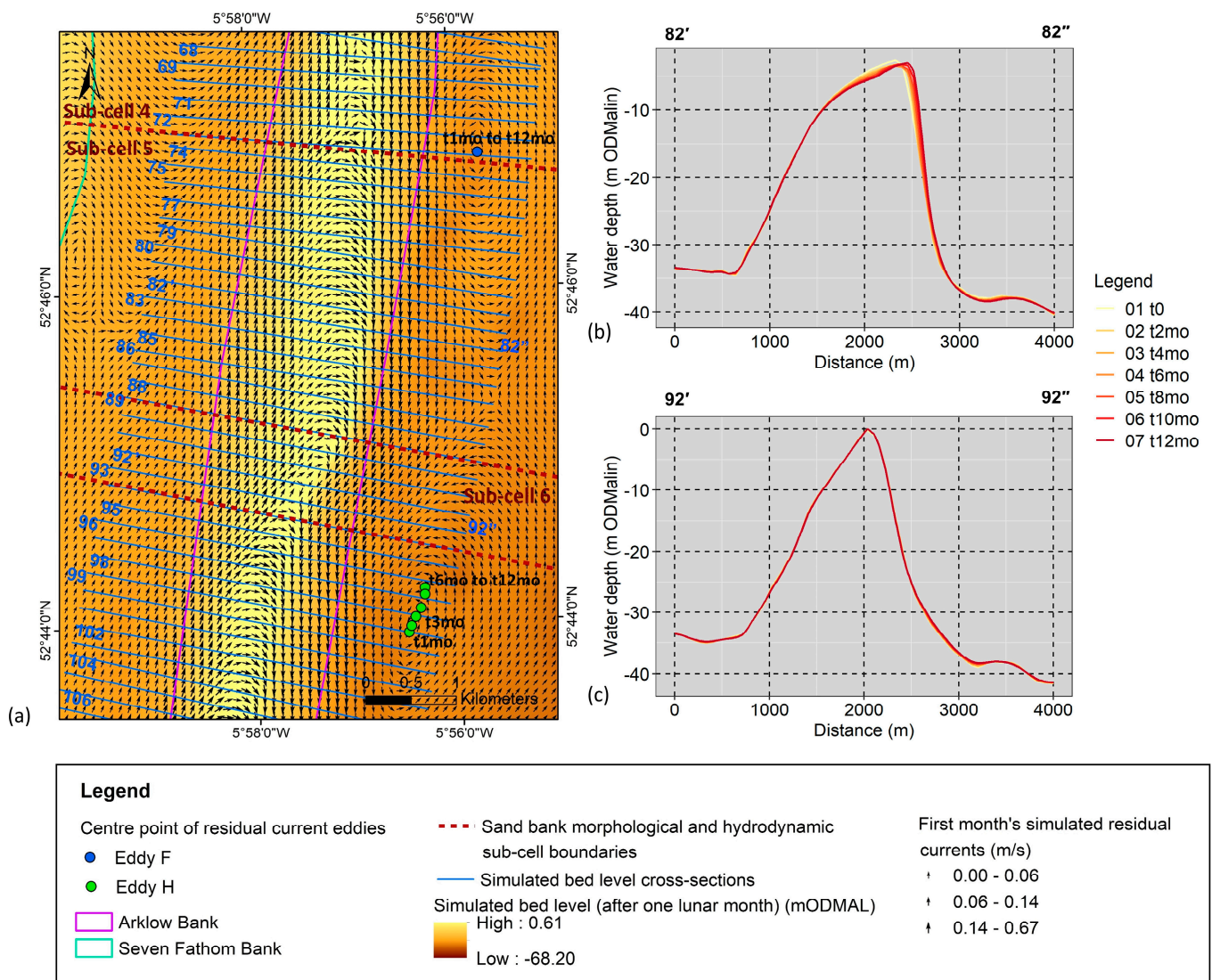


**Figure 10.** Morphodynamics and hydrodynamics at Sub-cells 5 and 6 of Arklow Bank. (a) Simulated bed level change after one lunar month and associated residual current vectors, overlain by the location of the centre point of residual eddies from residual currents during each subsequent lunar month simulation; ‘t6mo’ is the sixth lunar simulation month. (b,c) Simulated bed level over a one year simulation at cross-sections 82 and 92; ‘t0’ is the starting bed level, and ‘mo’ is subsequent months.

### 3.2.7. Sub-Cell 7

As the influence of the curvilinear flows from Eddy H on the upper bank is reduced, westward residual current flows dominate once again (Figure 11a). Westward migration of the upper bank dominates, but evidence of slowed migration and/or slight reversal in migration direction is shown in some areas, for example, cross-section L96 (Figure 11c). This may be related to the hydrodynamic–morphodynamic response described in other sub-cells of the bank, whereby a maximum slope threshold is reached, which modifies residual current flow dynamics, allowing bank rejuvenation of the bank through sediment accretion build up on the upper slopes and ultimately causing further hydrodynamic modification and a process re-start.

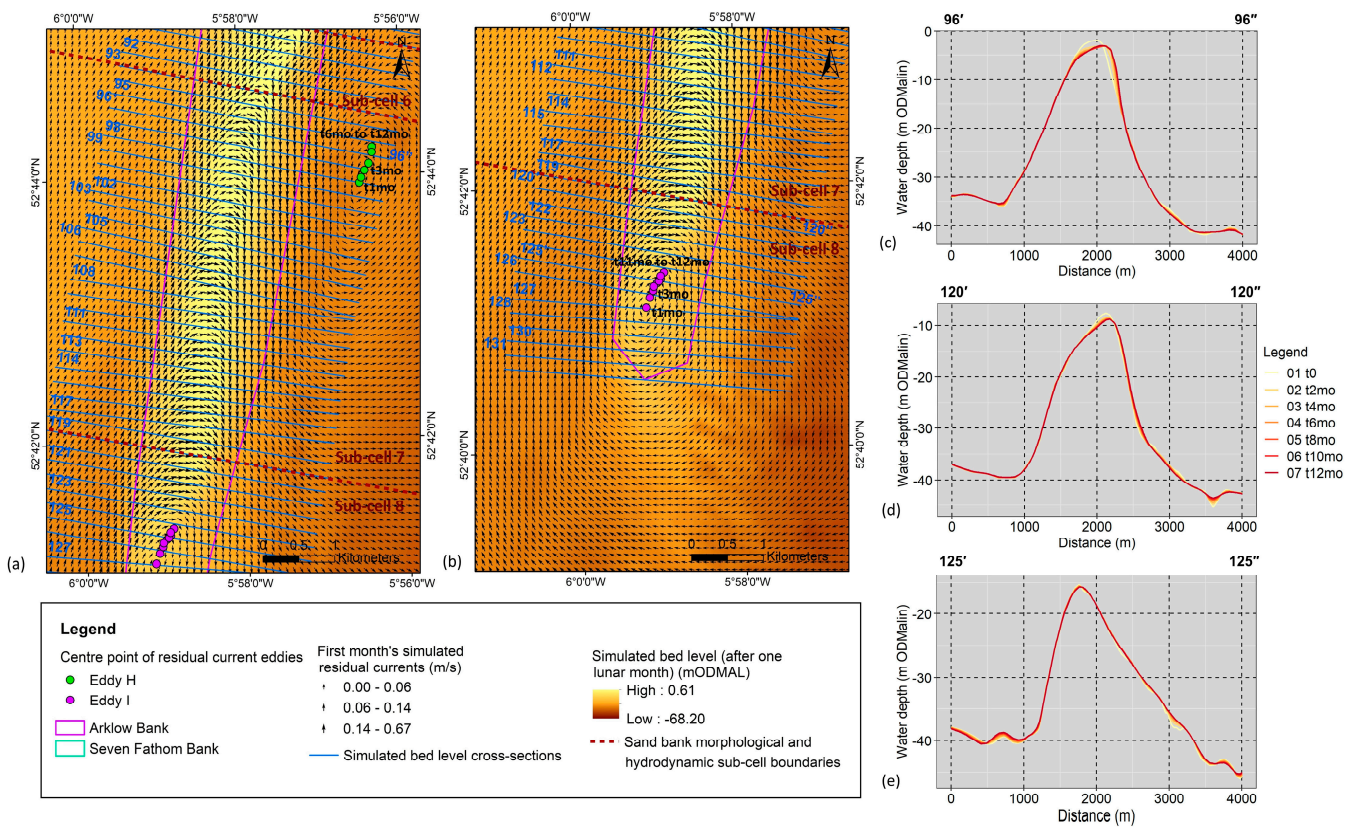


**Figure 11.** Morphodynamics and hydrodynamics at Sub-cells 7 and 8 of Arklow Bank. (a,b) Simulated bed level change after one lunar month and associated residual current vectors, overlain by the location of the centre point of residual eddies from residual currents during each subsequent lunar month simulation; ‘t6mo’ is the sixth lunar simulation month. (c–e) Simulated bed level over a one year simulation at cross-sections 96, 120 and 125; ‘t0’ is the starting bed level, and ‘mo’ is subsequent months.

### 3.2.8. Sub-Cell 8

Sub-cell 8 marks the transition of bank asymmetry from eastward to westward. This transition occurs over an approximate 700 m section of the bank (Figure 11b,d,e). The rest of Sub-cell 8 encompasses the tail of the bank, in which a westward asymmetry dominates. This aligns well with the existence of an anticlockwise residual current eddy over the southern extent of the bank, hereafter referred to as Eddy I, ultimately connecting the dominant southward flow on the eastern side of the bank with the northern flow on the western side of the bank (Figure 11b). The turning of the flows in an anticlockwise motion re-iterates a semi-closed sediment transport regime over the bank. This is combined with a residual current flow coming from the south-eastern side of the bank and pushing north-westward across the southern tip of the bank and connecting with the residual northward flow on the western side of the bank. This flow acts as an additional sediment source for the bank [7]. The centre point of Eddy I notably migrates approximately 350 m north-eastward from t1mo to t6mo, then 150 m in the same direction over the following 6-month period. The mobility of sediment along the southern extent of the bank is mainly in the form of bed load transport via sand waves [7].

### 3.3. Summary Discussion of Hydrodynamic Controls on Arklow Bank High Mobility and Bank Base Stability

As a result of the flood and ebb tidal dominance on the west and east side of the bank, respectively, an overall anticlockwise residual current eddy encompasses the bank, ultimately recycling sediment material within the bank cell. However, two different

phenomena play a role in controlling upper bank mobility and bank base stability: (i) off-bank anticlockwise residual eddies; (ii) on-bank hydrodynamic-morphodynamic response.

The positioning of multiple off-bank anticlockwise residual eddies both facilitate and inhibit east–west fluctuation of the bank and act as a control on long-term base stability. They do this in two ways: firstly, when the outer flows of the residual eddy on the eastern side of the bank are in a west to south-westward direction, these converge with residual eastward cross-flows coming from the western side of the bank. This generates a zone of absent or reduced residual cross-flow, inhibiting the mobility of the upper slopes of the bank and preserving bank base stability. Secondly, when outer flows of the residual eddy on the eastern side of the bank are in a south-east to eastward direction, these align with residual cross-flows coming from the western side of the bank instead of converging with them. This facilitates upper slope mobility.

In the case of this second mechanism, the control on the maximum limit or ‘threshold’ of east–west fluctuation, and thus base bank stability, is the on-bank hydrodynamic-morphodynamic feedback loop. This occurs in two forms:

7. a morphodynamic-hydrodynamic feedback loop allowing the generation of a conveyor belt of on-bank residual eddies and/or stationary transient residual eddies, continuously influencing east–west fluctuation of the bank;
8. the reduction and expansion of a residual current cross-flow, ultimately allowing the regeneration of the bank after a certain slope threshold has been reached.

The positioning of these off-bank anticlockwise residual current eddies on the outer edge of the larger anticlockwise eddy encompassing the entire bank facilitates sediment transfer in and out of the local morphological cell. An overview of each morphological sub-cell and the controlling hydrodynamic processes are summarised in Figure 12.

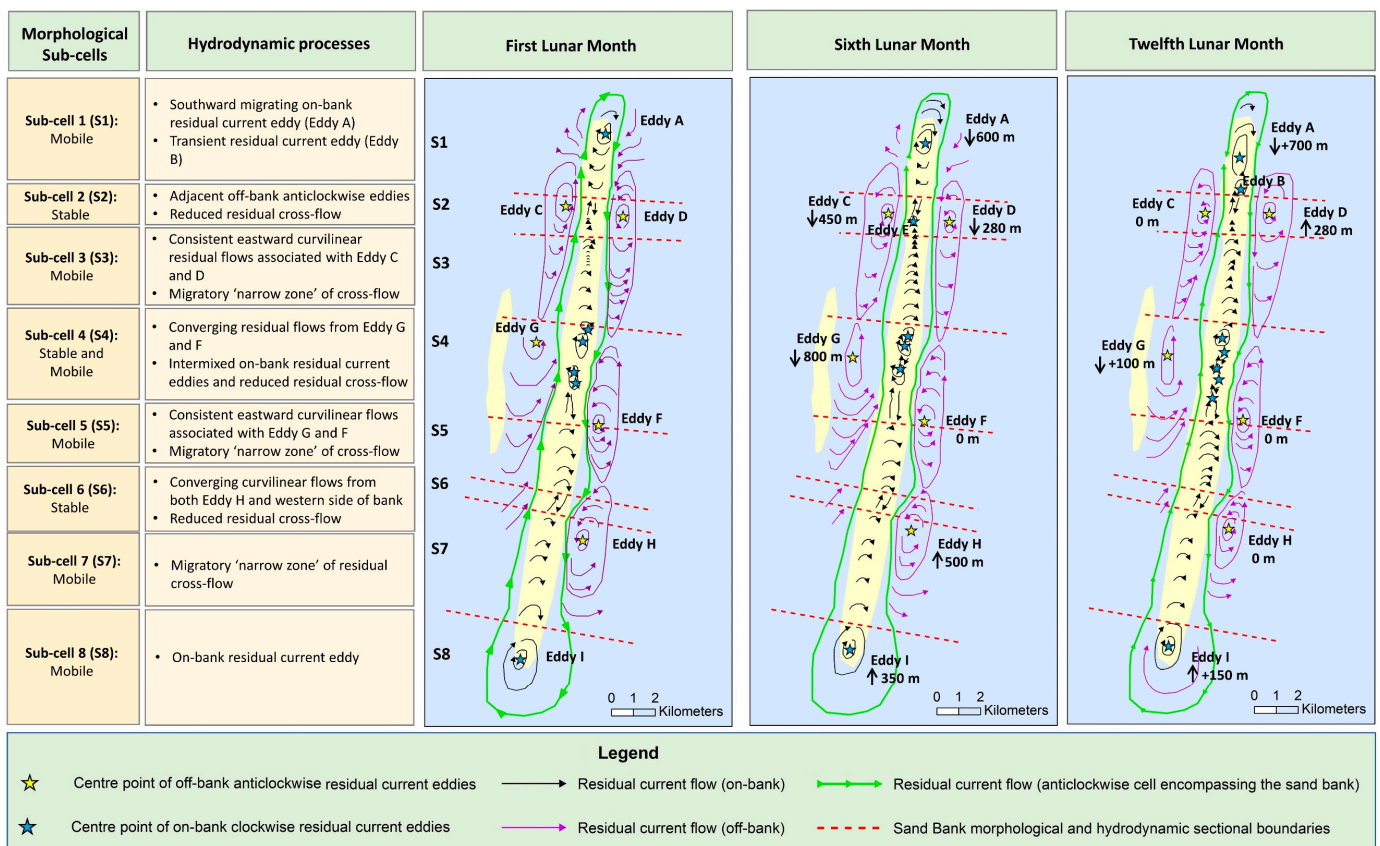


Figure 12. A schematic diagram summarising the hydrodynamic processes driving Arklow Bank’s upper slope mobility and bank base stability.

This new process-based understanding of Arklow Bank's complex hydrodynamic and morphodynamic regime can be used to guide the planning of offshore fieldwork to measure these morphological changes across the bank, thus improving the predictability of seabed level change in this region. This is crucial for the accurate and detailed design of OWF turbine foundations, cables and associated protection structures on and surrounding this bedform. Furthermore, by elucidating the baseline processes that maintain long-term seabed stability, this improves the ability to assess the risk of environmental instability due to future increased anthropogenic seabed disturbances in the south-western Irish Sea.

On a wider scale, this new comprehension of the hydrodynamic processes controlling bedform mobility has potential applicability to other offshore linear sand banks in tidally dominated shelf sea environments [8,22,34–36]. If proven similar, the outcomes of this study may re-define how these sand bank systems are analysed. Consequently, using similar methods as applied in this study to investigate the applicability of these controlling phenomena on other sand bank systems is imperative.

#### 4. Conclusions

This study uses a two-dimensional, dynamically coupled, hydrodynamic and sediment transport numerical model to investigate the hydrodynamic processes driving the morphodynamics of the offshore linear sand bank, Arklow Bank. Over a one-year simulation period, combined analysis of numerically modelled residual currents and bed levels elucidates the complex interconnected hydrodynamic and sediment transport regime in this area of the south-western Irish Sea. Ultimately, this study aims to define the hydrodynamic processes controlling morphodynamic variability and long-term stable positioning of Arklow Bank over time. The main conclusions drawn from this study are provided below.

9. A flood and ebb tidal dominance is evident on the west and east side of the bank, respectively, generating a residual anticlockwise tidal current eddy encompassing the entire bank. This ultimately recycles sediment material within the bank cell.
10. During an individual flood and ebb tide, sediment on the upper slopes is transported eastward and westward respectively along the full length of the bank due to the directional nature of tidal current cross-flow during these tidal phases. From a full semi-diurnal tidal cycle (divided into two flood and two ebb tidal phases) onwards, a variation in the direction of tidal asymmetry along the upper slopes of the bank is evident. This divides the bank into a variety of morphological sections migrating in different directions.
11. Eight unique sub-cells of the bank are identified, wherein a complex morphological-hydrodynamic feedback system is evident. These individual sub-cells display a variety of on-bank and off-bank hydrodynamic and morphological features, yet they fit together as one linear offshore sand bank, with high upper slope mobility and long-term bank base stability. The two main tidal phenomena that control upper bank mobility and bank base stability are (i) off-bank anticlockwise residual eddies and (ii) on-bank hydrodynamic-morphodynamic response.
12. The positioning of multiple off-bank anticlockwise residual current eddies on the edge of this cell is shown to influence east-west fluctuations of the upper slopes of the sand bank and act as a control of long-term stability. These off-bank eddies facilitate this type of movement when the outer flows of adjacent eddies, located on both sides of the bank, flow in a generally uniform direction. Whereas they inhibit this east-west movement when the outer flows of adjacent eddies, on either side of the bank, flow in converging directions towards the bank itself. Off-bank anticlockwise eddies also facilitate sediment transport in and out of the local morphological cell.
13. The control of the maximum limit of upper bank east-west fluctuation is the on-bank hydrodynamic-morphodynamic feedback loop through (i) the formation of migratory and stationary transient on-bank clockwise residual tidal current eddies and (ii) the formation of transient 'narrow' residual tidal current cross-flow zones.

14. The concept of a ‘threshold slope angle’ is also introduced. When the upper slopes of the bank reach a certain threshold angle, a hydrodynamic response is stimulated that reverses upper bank migration in the opposite direction. By taking into consideration this concept in conjunction with the identified controlling hydrodynamic processes, analysis of this system at a higher temporal scale and over a longer time period could help determine the maximum limits of vertical and horizontal bed level changes along the bank, as well as the rate and frequency at which these limits are reached. The information provided in this study can be used to guide offshore survey planning for existing and planned OWF projects in order to measure these morphological changes on Arklow Bank. The details provided in this study can reduce costs for such an expedition.
15. The new process-based understanding of Arklow Bank’s complex hydrodynamic and morphodynamic regime introduced in this study aids the predictability of future seabed level changes in this highly mobile sand-dominated environment. Where the maximum bed level change over a one-month period along the bank is +7.3 m to −3.4 m, the magnitude and rate of bed level change varies hugely along the length of the bank. This highlights the need for careful selection of scour and bed level change mitigation strategies for each potential wind turbine generator (WTG) position. Resultingly, the information provided in this study not only informs offshore geophysical survey design to confirm these modelled morphological changes but also informs concept layout design and foundation design.
16. This comprehension of Arklow Bank’s morphodynamic system has the potential to re-define how we analyse offshore linear sand banks. Consequently, the methods used in this study should be applied to offshore linear sand banks in other tidally dominated environments to investigate this wider connection.

**Supplementary Materials:** The following supporting information can be downloaded at: <https://www.mdpi.com/article/10.3390/geosciences13020060/s1>, File S1.

**Author Contributions:** Conceptualization, S.C., M.O. and J.M.; Formal analysis, S.C.; Investigation, S.C. and M.C.; Methodology, S.C.; Supervision, M.O., M.C. and J.M.; Writing—original draft, S.C.; Writing—review & editing, S.C., M.O., M.C. and J.M. All authors have read and agreed to the published version of the manuscript.

**Funding:** S.C. is funded by the Irish Research Council (IRC) through grant EBPPG/2019/158 (Employment-Based Postgraduate Programme Scholarship). M.C. is funded under an Irish Research Council Enterprise Partnership Scheme Postdoctoral Fellowship (EPSPD/2020/109) and in part by a research grant from Science Foundation Ireland (SFI) under Grant Number 13/RC/2092, with support from Gavin and Doherty Geosolutions Ltd. and the Geological Survey of Ireland (GSI). This project benefitted from funded industry–academic collaboration involving Gavin and Doherty Geosolutions, University College Dublin (iCRAG) and University College Cork (MaREI), supported by the Marine Institute under the Marine Research Programme 2014–2020 (Grant-Aid Agreement No. IND/18/18). Ship time on the RV Celtic Voyager was funded by the Marine Institute through the 2020–2021 ship-time programme under the National Marine Research and Innovation Strategy 2017–2021.

**Informed Consent Statement:** Not applicable.

**Data Availability Statement:** The bathymetry data used in Figures 1, 2 and 4 is sourced from INFOMAR (<https://www.infomar.ie/>, (accessed on 20 March 2020)), and EMODnet Bathymetry Consortium [27]. The set-up and validation of the numerical model described in Section 2 is provided as Supplementary Material to this paper.

**Acknowledgments:** The authors would gratefully like to acknowledge the Mobility of Sediment Waves and Sand Banks in the Irish Sea (MOVE) (CV20010, CV20036 and CV21035) shipboard crew and scientists, and onshore Marine Institute and INFOMAR support personnel for assistance with data acquisition.

**Conflicts of Interest:** The authors declare no conflict of interest.

## References

1. Ellis, J.R.; Maxwell, T.; Schratzberger, M.; Rogers, S.I. The Benthos and Fish of Offshore Sandbank Habitats in the Southern North Sea. *J. Mar. Biol. Assoc. United Kingd.* **2011**, *91*, 1319–1335. [\[CrossRef\]](#)
2. Sell, A.F.; Kröncke, I. Correlations between Benthic Habitats and Demersal Fish Assemblages—A Case Study on the Dogger Bank (North Sea). *J. Sea Res.* **2013**, *80*, 12–24. [\[CrossRef\]](#)
3. van Dijk, T.A.G.P.; van Dalssen, J.A.; Van Lancker, V.; van Overmeeren, R.A.; van Heteren, S.; Doornenbal, P.J. Benthic Habitat Variations over Tidal Ridges, North Sea, the Netherlands. In *Seafloor Geomorphology as Benthic Habitat*; Harris, P.T., Baker, E.K., Eds.; Elsevier: London, UK, 2012; pp. 241–249. [\[CrossRef\]](#)
4. Velegrakis, A.F.; Ballay, A.; Poulos, S.; Radzevičius, R.; Bellec, V.; Manso, F. European Marine Aggregates Resources: Origins, Usage, Prospecting and Dredging Techniques. *J. Coast. Res.* **2010**, 1–14. [\[CrossRef\]](#)
5. Wyns, L.; Roche, M.; Barette, F.; Van Lancker, V.; Degrendele, K.; Hostens, K.; De Backer, A. Near-Field Changes in the Seabed and Associated Macrobenthic Communities Due to Marine Aggregate Extraction on Tidal Sandbanks: A Spatially Explicit Bio-Physical Approach Considering Geological Context and Extraction Regimes. *Cont. Shelf Res.* **2021**, *229*, 104546. [\[CrossRef\]](#)
6. RPS. *Arklow Bank Wind Park Phase 2 Offshore Infrastructure: Environmental Impact Assessment Report—Appendix 3.1: Consultation Report*; Sure Partners Ltd.: Dublin, Ireland, 2021.
7. Creane, S.; Coughlan, M.; O’Shea, M.; Murphy, J. Development and Dynamics of Sediment Waves in a Complex Morphological and Tidal Dominant System: Southern Irish Sea. *Geosciences* **2022**, *12*, 431. [\[CrossRef\]](#)
8. Dyer, K.R.; Huntley, D.A. The Origin, Classification and Modelling of Sand Banks and Ridges. *Cont. Shelf Res.* **1999**, *19*, 1285–1330. [\[CrossRef\]](#)
9. Bradley, S.L.; Milne, G.A.; Shennan, I.; Edwards, R. An Improved Glacial Isostatic Adjustment Model for the British Isles. *J. Quat. Sci.* **2011**, *26*, 541–552. [\[CrossRef\]](#)
10. Scourse, J.D.; Ward, S.L.; Wainwright, A.; Bradley, S.L.; Uehara, K. The Role of Megatides and Relative Sea Level in Controlling the Deglaciation of the British–Irish and Fennoscandian Ice Sheets. *J. Quat. Sci.* **2018**, *33*, 139–149. [\[CrossRef\]](#)
11. Uehara, K.; Scourse, J.D.; Horsburgh, K.J.; Lambeck, K.; Purcell, A.P. Tidal Evolution of the Northwest European Shelf Seas from the Last Glacial Maximum to the Present. *J. Geophys. Res.: Ocean.* **2006**, *111*, 1–15. [\[CrossRef\]](#)
12. Ward, S.L.; Neill, S.P.; Scourse, J.D.; Bradley, S.L.; Uehara, K. Sensitivity of Palaeotidal Models of the Northwest European Shelf Seas to Glacial Isostatic Adjustment since the Last Glacial Maximum. *Quat. Sci. Rev.* **2016**, *151*, 198–211. [\[CrossRef\]](#)
13. Creane, S.; O’Shea, M.; Coughlan, M.; Murphy, J. The Irish Sea Bed Load Parting Zone: Is It a Mid-Sea Hydrodynamic Phenomenon or a Geological Theoretical Concept? *Estuar. Coast. Shelf Sci.* **2021**, *263*, 107651. [\[CrossRef\]](#)
14. Coughlan, M.; Guerrini, M.; Creane, S.; O’Shea, M.; Ward, S.L.; Van Landeghem, K.J.J.; Murphy, J.; Doherty, P. A New Seabed Mobility Index for the Irish Sea: Modelling Seabed Shear Stress and Classifying Sediment Mobilisation to Help Predict Erosion, Deposition, and Sediment Distribution. *Cont. Shelf Res.* **2021**, *229*, 104574. [\[CrossRef\]](#)
15. Van Landeghem, K.J.J.; Baas, J.H.; Mitchell, N.C.; Wilcockson, D.; Wheeler, A.J. Reversed Sediment Wave Migration in the Irish Sea, NW Europe: A Reappraisal of the Validity of Geometry-Based Predictive Modelling and Assumptions. *Mar. Geol.* **2012**, *295–298*, 95–112. [\[CrossRef\]](#)
16. Van Landeghem, K.J.J.; Uehara, K.; Wheeler, A.J.; Mitchell, N.C.; Scourse, J.D. Post-Glacial Sediment Dynamics in the Irish Sea and Sediment Wave Morphology: Data-Model Comparisons. *Cont. Shelf Res.* **2009**, *29*, 1723–1736. [\[CrossRef\]](#)
17. Van Landeghem, K.J.J.; Wheeler, A.J.; Mitchell, N.C.; Sutton, G. Variations in Sediment Wave Dimensions across the Tidally Dominated Irish Sea, NW Europe. *Mar. Geol.* **2009**, *263*, 108–119. [\[CrossRef\]](#)
18. Panigrahi, J.K.; Ananth, P.N.; Umesh, P.A. Coastal Morphological Modeling to Assess the Dynamics of Arklow Bank, Ireland. *Int. J. Sediment Res.* **2009**, *24*, 299–314. [\[CrossRef\]](#)
19. Wentworth, C.K. A Scale of Grade and Class Terms for Clastic Sediments. *J. Geol.* **1922**, *30*, 377–392. [\[CrossRef\]](#)
20. Harris, J.M.; Whitehouse, R.J.S.; Sutherland, J. Marine Scour and Offshore Wind—Lessons Learnt and Future Challenges. In Proceedings of the International Conference on Offshore Mechanics and Arctic Engineering-OMAE, Rotterdam, The Netherlands, 19–24 June 2011; Volume 5, pp. 849–858. [\[CrossRef\]](#)
21. Whitehouse, R.J.S.; Harris, J.M.; Sutherland, J.; Rees, J. The Nature of Scour Development and Scour Protection at Offshore Windfarm Foundations. *Mar. Pollut. Bull.* **2011**, *62*, 73–88. [\[CrossRef\]](#)
22. Park, H.; Vincent, C.E. Evolution of Scroby Sands in the East Anglian Coast, UK. *J. Coast. Res.* **2007**, 868–873.
23. Horrillo-Caraballo, J.M.; Yin, Y.; Fairley, I.; Karunarathna, H.; Masters, I.; Reeve, D.E. A Comprehensive Study of the Tides around the Welsh Coastal Waters. *Estuar. Coast. Shelf Sci.* **2021**, *254*, 107326. [\[CrossRef\]](#)
24. Harris, P.T.; Pattiaratchi, C.B.; Collins, M.B.; Dalrymple, R.W. What Is a Bedload Parting? In *Tidal Signatures in Modern and Ancient Sediments*; Flemming, B.W., Bartholoma, A., Eds.; Blackwell: Oxford, UK. [\[CrossRef\]](#)
25. Pingree, R.D.; Griffiths, D.K. Sand Transport Paths around the British Isles Resulting from M2 and M4 Tidal Interactions. *J. Mar. Biol. Assoc. United Kingd.* **1979**, *59*, 497–513. [\[CrossRef\]](#)
26. Pugh, D.T. Tidal Amphidrome Movement and Energy Dissipation in the Irish Sea. *Geophys. J. R. Astron. Soc.* **1981**, *67*, 515–527. [\[CrossRef\]](#)
27. EMODnet Bathymetry Consortium. EMODnet Digital Bathymetry (DTM 2020). 2020. Available online: <https://doi.org/10.12770/bb6a87dd-e579-4036-abe1-e649cea9881a> (accessed on 20 March 2020).

28. Roetert, T.; Raaijmakers, T.; Borsje, B. Cable Route Optimization for Offshore Wind Farms in Morphodynamic Areas. In Proceedings of the 27th International Offshore and Polar Engineering Conference, San Francisco, CA, USA, 25 June 2017; pp. 595–606.
29. Fazeres-Ferradosa, T.; Chambel, J.; Taveira-Pinto, F.; Rosa-Santos, P.; Taveira Pinto, F.V.C.; Giannini, G.; Haerens, P. Scour Protections for Offshore Foundations of Marine Energy Harvesting Technologies: A Review. *J. Mar. Sci. Eng.* **2021**, *297*. [[CrossRef](#)]
30. DHI Group. *MIKE 21 & MIKE 3 Flow Model FM Sand Transport Module Scientific Documentation*; DHI Water & Environment: Brisbane, Australia, 2017.
31. DHI Group. *MIKE 21 Flow Model: Hydrodynamic Module User Guide*; DHI Water & Environment: Brisbane, Australia, 2017.
32. Creane, S.; O'Shea, M.; Coughlan, M.; Murphy, J. Estimation of Suspended Solids Concentration from Acoustic Doppler Current Profiler in a Tidally-Dominated Continental Shelf Sea Setting and Its Use as a Numerical Modelling Validation Technique. *Coast. Eng.* **2022**, *14*, 53027–53037.
33. EMODnet Geology. Seabed Substrates. Available online: <https://www.emodnet-geology.eu/data-products/seabed-substrates/> (accessed on 10 April 2022).
34. Johnson, M.A.; Kenyon, N.H.; Belderson, R.H.; Stride, A.H. Sand Transport. In *Offshore Tidal Sands: Processes and Deposits*; Stride, A.H., Ed.; Chapman and Hall: London, UK, 1982; pp. 58–94. [[CrossRef](#)]
35. Collins, M.B.; Shimwell, S.J.; Gao, S.; Powell, H.; Hewitson, C.; Taylor, J.A. Water and Sediment Movement in the Vicinity of Linear Sandbanks: The Norfolk Banks, Southern North Sea. *Mar. Geol.* **1995**, *123*, 125–142. [[CrossRef](#)]
36. Stride, A.H. Offshore Tidal Deposits: Sand Sheet and Sand Bank Facies. In *Offshore Tidal Sands: Processes and Deposits*; Stride, A.H., Ed.; Springer: Dordrecht, The Netherlands, 1982; pp. 95–125. [[CrossRef](#)]

**Disclaimer/Publisher's Note:** The statements, opinions and data contained in all publications are solely those of the individual author(s) and contributor(s) and not of MDPI and/or the editor(s). MDPI and/or the editor(s) disclaim responsibility for any injury to people or property resulting from any ideas, methods, instructions or products referred to in the content.